Numerical analysis of circular core shaped photonic crystal fiber for orbital angular momentum with efficient transmission

Md. Mehedi Hassan[1] · Md. Anowar Kabir[1] · Md. Nadim Hossain[1] · Truong Khang Nguyen[4,5] · Bikash Kumar Paul[1,2,3] · Kawsar Ahmed[1,2] · Vigneswaran Dhasarathan[4,5]

Abstract
In this paper, a circular core shaped photonic crystal fiber (PCF) is proposed and the optical propagation characteristics are investigated and simulated by applying the finite element method (FEM) with the help of COMSOL Multiphysics software. The cladding of this PCF is composed of fused silica including a large center air-hole. The simulation process is performed within 1000–2000 nm wavelength. The raised PCF supports up to 38 OAM modes with larger bandwidth (1000 nm) as well as flat dispersion variations. The refractive index difference can exceed 10^{-4} for each OAM mode. The confinement loss of this PCF remains low approximately around 10^{-9} to 10^{-8} dB/m, comparatively better the nonlinearity, the numerical aperture, and the dispersion variation evolves into smoother. So, all these optimizing optical properties prove that our designed PCF is a promising candidate for the OAM mode transmission and other relevant optical communications.

1 Introduction

In the twenty-first century, communication technology is developed rapidly by photonic crystal fiber (PCF). In this era of communication technology, time-division multiplexing (TDM), dense mode-division multiplexing (DMDM), and space division multiplexing (SDM) are developed and enriched with increasing the capacity of transmission. But the SDM is a popular and attractive method to overcome the capacity limit of optical communication [1, 2]. Orbital angular momentum (OAM) is a promising candidate for the

✉ Vigneswaran Dhasarathan
vigneswaran.d@tdtu.edu.vn

1 Department of Information and Communication Technology, Mawlana Bhashani Science and Technology University, Santosh, Tangail 1902, Bangladesh

2 Group of Bio-photomatiχ, Mawlana Bhashani Science and Technology University, Santosh, Tangail 1902, Bangladesh

3 Department of Software Engineering, Daffodil International University, Sukrabad, Dhanmondi, Dhaka 1207, Bangladesh

4 Division of Computational Physics, Institute for Computational Science, Ton Duc Thang University, Ho Chi Minh City, Vietnam

5 Faculty of Electrical and Electronics Engineering, Ton Duc Thang University, Ho Chi Minh City, Vietnam

SDM [3]. It provides some important features to improve fiber communication strategy. In 1992, the OAM techniques of optics were widely recognized by Allen via Lager Gaussian beams at first [4]. The OAM beams have two ordinary characteristics of eddy wavefront and rounded field power distribution. It is expressed by $e^{(il\varphi)}$. Where, l (....., − 3, − 2, − 1, 0, + 1, + 2, + 3,.....) is the topological accusation and φ is the angle of azimuth [5]. Recently, the OAM beams are generated by some strategy. This method uses cylindrical lenses [6], spiral plates [7], diffractive optical elements [8, 9]. The number of OAM modes is an important property for optical communication. Thus, we need to compose new structures of fiber to increase transmission capacity and support higher OAM modes.

The act of OAM transporting is sustained by circular PCF [1], dual guided ring-core PCF [2], spiral PCF [10], circular PCF with a square hole [11], etc. These are separately good for confinement loss, nonlinearity, numerical aperture (NA) and, dispersion. The robust transmission and communication capacity are increased by a higher number of OAM modes. Zhang et al. [3] proposed a C-PCF supporting 26 OAM mode. Jia et al. [5] proposed a hollow-core ring PCF supporting 38 OAM mode. Nevertheless, it was not enough for an efficient communication system. Thus, it is imperative to design a special PCF that supports more OAM mode. It also supports the robust transmission with low confinement

loss, low dispersion variation, high refractive index differences, better nonlinearity, and numerical aperture.

This article proposed a circular photonic crystal fiber with a special design of air holes in the cladding region. This PCF supports up to 38 OAM modes with 1000 nm bandwidth. The highest refractive index difference is 4.899×10^{-2} at 2000 nm wavelength for $|HE_{11,1}-EH_{9,1}|$. Besides, low confinement loss, smooth dispersion curve, convenient nonlinear coefficients, and relatively better numerical aperture are obtained from the proposed PCF. Benefitting from these properties, the raised PCF could be a strong candidate for the transmission scheme.

2 Design strategy and theoretical analysis

The basic structure of the proposed PCF is shown clearly in Fig. 1 with a little physical explanation. The proposed PCF is composed of a large center air-hole and the three-layer well-shaped circular air holes in the cladding region which enhanced the performance of the PCF. In the designed PCF, the radius of the center air-hole is $r_3 = 4.00$ μm. The large center air-hole is favorable for the high number of OAM modes. Also, the radius of the inner and outer circle is $r_1 = 17.5$ μm and $r_2 = 16$ μm, respectively. Thus, the width of the perfectly matched layer (PML) is 1.5 μm or 8.5714% which should maintain the manner of the boundary condition (less or equal 10%). The PML reduces the undesirable immaterial scattering. The diameter of the air holes in the cladding region is 2 μm and the pitch (distance between adjacent circles, Λ) is 2.5 μm. The air holes of the raised PCF are built by the circle through the COMSOL Multiphysics 4.3b software.

The light leakage of the PCF is reduced by the well-structured layer of air holes. The design and simulation of the proposed PCF are done by the COMSOL Multiphysics software. All numerical analyses and simulated calculations are performed by the finite element method (FEM). By performing the simulation on the proposed PCF, some PCF properties are calculated. These are an effective refractive index difference (ERID), dispersion variation, effective area, confinement loss, nonlinearity, and numerical aperture.

The fused silica is used as the background material. The refractive index (RI) of fused silica is 1.446 at the wavelength of 1.55 μm [12]. The flat dispersion is influenced by the lower effective refractive index. Thus, the fused silica is the best for this parameter. The RI of the background material is evaluated by the Sellmeier equation Eq. (1) [13]:

$$n^2(\lambda) = 1 + \sum_{i=1}^{3} \frac{A_i \lambda^2}{\lambda^2 - \lambda_i^2}, \tag{1}$$

where λ_i^2 and A_i are the Sellmeier coefficient and $n(\lambda)$ is the RI that varies with the wavelength.

The ERID of the OAM mode can be calculated through Eq. (2) and it is symbolized by Δn_{eff}:

$$\Delta n_{\text{eff}} = \left| n_{\text{eff}_{HE_{l+1,1}}} - n_{\text{eff}_{EH_{l-1,1}}} \right| > 10^{-4}. \tag{2}$$

The waveguide dispersion is expressed by Eq. (3) [10]:

$$D = -\frac{1}{\lambda c} \left(\lambda^2 \frac{d^2 \text{Re}[n_{\text{eff}}]}{d\lambda^2} \right), \tag{3}$$

where λ is the wavelength, c is the velocity of light in the free space (3×10^8 m s^{-1}) and $\text{Re}[n_{\text{eff}}]$ is the real part of the effective RI.

The confinement loss (C_{loss}) is induced by internal material absorption of light and waveguide geometry. The C_{loss} can be expressed by Eq. (4) [11]:

$$C_{\text{loss}} = \frac{40\pi}{\ln(10)\lambda} \text{Im}(n_{\text{eff}})(\text{dB/m}), \tag{4}$$

where λ is the operating wavelength and $\text{Im}(n_{\text{eff}})$ is the imaginary part of the RI.

The effective area of the OAM mode is characterized by A_{eff} and can be figured by the mathematical Eq. (5) [14]:

$$A_{\text{eff}} = \frac{\left\{ \left(\iint |E(x,y)|^2 dxdy \right) \right\}^2}{\iint |E(x,y)|^4 dxdy}, \tag{5}$$

where $E(x,y)$ is an electric-field distribution of the electromagnetic transverse field.

Numerical aperture is the entire capacity of gathering beam in optical fiber. It is evaluated by Eq. (6) [14]:

$$NA = \frac{1}{\sqrt{1 + \frac{\pi A_{\text{eff}}}{\lambda^2}}}. \tag{6}$$

PML
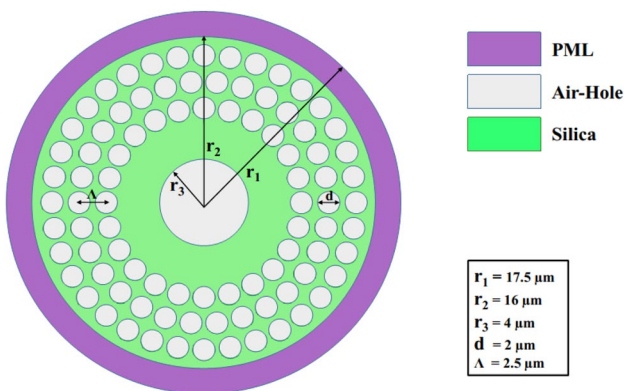Air-Hole
Silica

$r_1 = 17.5$ μm
$r_2 = 16$ μm
$r_3 = 4$ μm
$d = 2$ μm
$\Lambda = 2.5$ μm

Fig. 1 The cross-sectional view of the proposed C-PCF

The nonlinearity of the PCF is symbolized by the γ and it is expressed by the Eq. (7) [15]:

$$\gamma = \frac{2\pi n_2}{\lambda A_{\text{eff}}},\tag{7}$$

where $n_2 = 2.3 \times 10^{-20}$ m^2 W^{-1} [16] denotes the nonlinear index of fused silica.

3 Results, discussion and analysis

In this section, we have widely described some OAM parameters such as the supported OAM modes for the proposed PCF, ERID, dispersion profile, confinement loss, effective refractive area, numerical aperture, and nonlinearity with proper diagram, equation, and discussion.

3.1 The supported OAM modes for the proposed PCF

The proposed PCF supports up to 38 OAM modes with the wavelength ranging from 1000 to 2000 nm. In addition, a center air-hole area, air-hole pattern in the cladding region also effects to produces the OAM mode. The large center air-hole, ring number, and well-organized air holes in the cladding of the PCF help to increase the OAM mode number because it acquired adequate space to produces the OAM mode as well as it reduces the light leakage in the cladding region. Besides, from the experiment, the raised PCF supports up to 38 OAM modes within the 1000 to 2000 nm wavelength. The intensity and phase are used in multiplexing. It also ensures the robust transmission of data. The number of OAM modes is calculated through Eqs. (8) and (9) [15]:

$$\left\{ \begin{array}{l} \text{OAM}_{\pm l,1}^{\pm} = \text{HE}_{l+1,1}^{\text{even}} \pm j\text{HE}_{l+1,1}^{\text{odd}} \\ \text{OAM}_{\pm l,1}^{\mp} = \text{EH}_{l-1,1}^{\text{even}} \pm j\text{EH}_{l-1,1}^{\text{odd}} \end{array} \right\} \quad ;(l > 1)\tag{8}$$

$$\left\{ \begin{array}{l} \text{OAM}_{\pm 1,1}^{\pm} = \text{HE}_{2,1}^{\text{even}} \pm j\text{HE}_{2,1}^{\text{odd}} \\ \text{OAM}_{\pm 1,1}^{\mp} = \text{TM}_{0,1} \pm j\text{TE}_{0,1} \end{array} \right\} \quad ;(l = 1),\tag{9}$$

where l is the topological charge and radial order is equal to 1 for the OAM mode calculation. Accidental degeneracies are occurred by the higher-order [17]. It is a challenge for the multiplexing scheme. All of the OAM modes for the designed PCF are given bellow:
OAM$_{\pm 1,1}^{\pm}$(HE$_{2,1}$), OAM$_{\pm 2,1}^{\pm}$(HE$_{3,1}$, EH$_{1,1}$), OAM$_{\pm 3,1}^{\pm}$(HE$_{4,1}$, EH$_{2,1}$), OAM$_{\pm 4,1}^{\pm}$(HE$_{5,1}$, EH$_{3,1}$), OAM$_{\pm 5,1}^{\pm}$(HE$_{6,1}$, EH$_{4,1}$), OAM$_{\pm 6,1}^{\pm}$(HE$_{7,1}$, EH$_{5,1}$), OAM$_{\pm 7,1}^{\pm}$(HE$_{8,1}$, EH$_{6,1}$), OAM$_{\pm 8,1}^{\pm}$(HE$_{9,1}$, EH$_{7,1}$), OAM$_{\pm 9,1}^{\pm}$(HE$_{10,1}$, EH$_{8,1}$), OAM$_{\pm 10,1}^{\pm}$(HE$_{11,1}$, EH$_{9,1}$).

The intensity of the OAM mode is obtained by the electromagnetic wave of x component and phase for including argument function. Some of them are shown in Fig. 2. The intensity and phase of the proposed PCF are achieved by choosing a rainbow color from the color table in the simulation software (COMSOL Multiphysics). We know that the effective refractive index (RI) of HE mode is lower than EH modes for the same order OAM modes at the same wavelength. So, discrimination between HE and EH modes appeared at the time of simulation of the raised PCF in the COMSOL Multiphysics software. Since the refractive index (RI) of the background material (silica) is higher than the center large air-hole, therefore OAM modes will be propagated between the center air-hole and air-holes pattern of the cladding region. Therefore, the gap between center air-hole and air-holes pattern of the cladding region is also called the light-guiding area or core of the raised PCF. The same phenomenon was displayed through recently published articles [1, 14, 15].

The intensity of Fig. 2a–g shows the different OAM modes with two different colors. The OAM as a multiplexing system in digital communication is transmitted maximum (1) or minimum (0) types of multiple data at a time. For intensity, two colors are indicator and phase separator of two types of data. Two colors are separated by an angle. This angle is changed by varying the number of OAM modes. For example, in mode of EH$_{6,1}$, the angle between one color to another color is 30° because of 12 (6 + 6) data are transmitted. For mode of HE$_{8,1}$, the angle between one color to another color is 22.5° because of 16 (8 + 8) data are transmitted here. Besides, the phase distribution is separated by one color. This color is not same as the color of intensity; it is a random selection from color table at the time of simulation. Both TE$_{0,1}$ and TM$_{0,1}$ given in Fig. 2i, j are the types of two vector modes that approve us to construct OAM modes with topological charge $l = 1$. The red arrows in Fig. 2 indicate the vector notations of the OAM mode [10].

3.2 Effective refractive index differences (ERIDs)

The ERID is the absolute value of differences between HE and EH mode. It is calculated mathematically through Eq. (2). It is shown in Fig. 3 and the pinkie straight line 10^{-4} is used as a reference. In Fig. 3, the ERID of any OAM is greater than 10^{-4} over the wavelength from 1000 to 2000 nm. It can be achieved for a big index difference between silica cladding and hollow air-hole. Thus, each mode propagates independently in an effective way and it also prevents a couple of linear polarization (LP) of the contiguous vector modes. Here, it is also observed that Δn_{eff} is higher for the higher group of OAM modes except for OAM$_{3,1}$ mode and as well as Δn_{eff} increases with raising the wavelength.
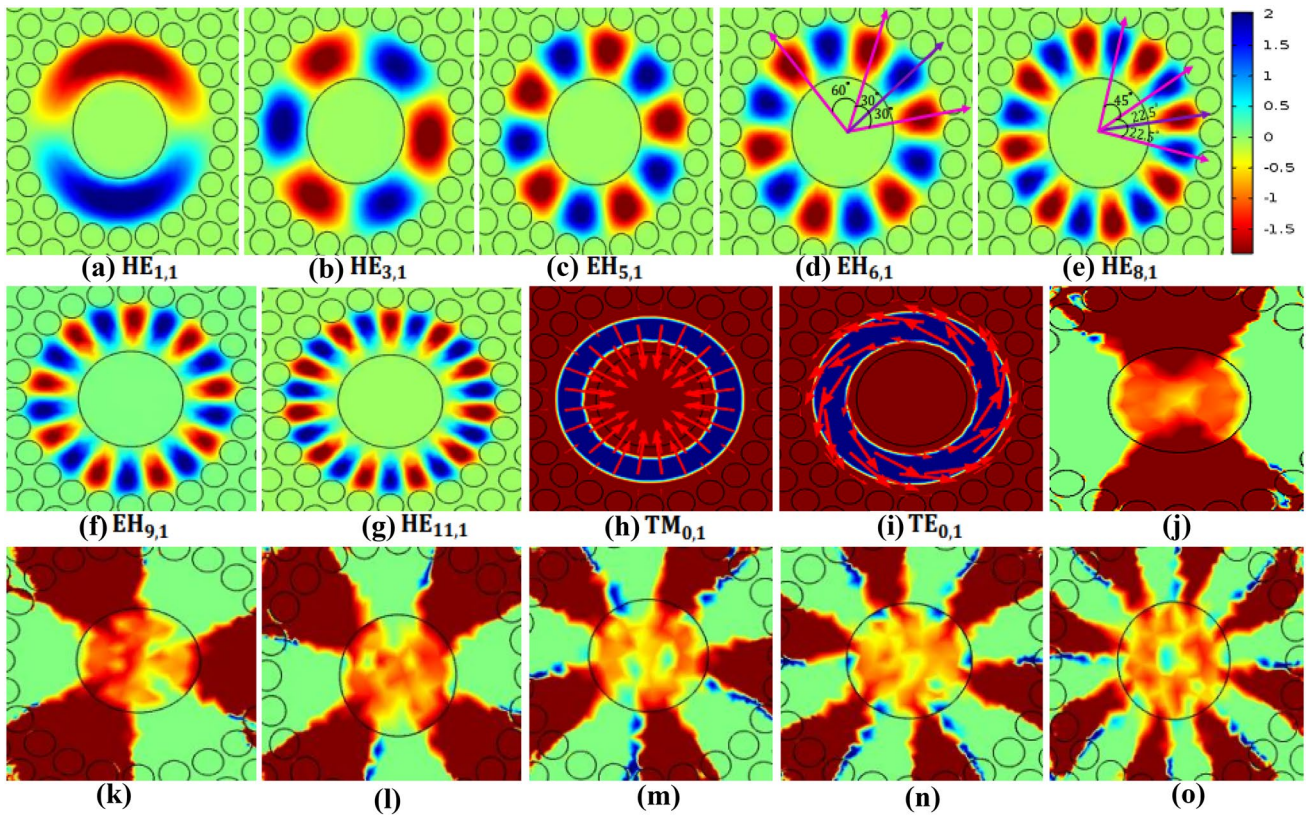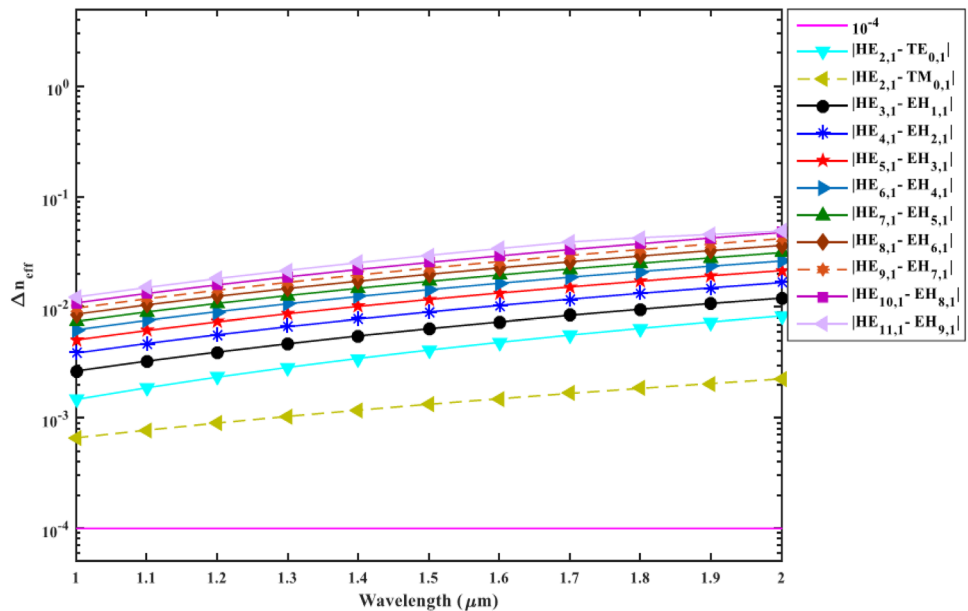
(a) $HE_{1,1}$ **(b)** $HE_{3,1}$ **(c)** $EH_{5,1}$ **(d)** $EH_{6,1}$ **(e)** $HE_{8,1}$

(f) $EH_{9,1}$ **(g)** $HE_{11,1}$ **(h)** $TM_{0,1}$ **(i)** $TE_{0,1}$ **(j)**

(k)   **(l)**   **(m)**   **(n)**   **(o)**

Fig. 2 **a–i** The intensity of some OAM modes and **j–o** phase of $HE_{2,1}$, $HE_{3,1}$, $EH_{4,1}$, $HE_{5,1}$, $EH_{6,1}$, and $EH_{8,1}$ OAM modes

Fig. 3 ERID of the different OAM modes versus operating wavelength

3.3 Dispersion profile

The dispersion and ERID are affected by the real value of RI. There are two types of dispersion: material dispersion and waveguide dispersion. The material dispersion has little effect on total dispersion. So, we focused only on the waveguide dispersion. The dispersion is calculated according to Eq. (3) and it is displayed in Fig. 4. It is noted that the dispersion of the operating last two-wavelength is discarded. It has occurred for the second-order derivation as the
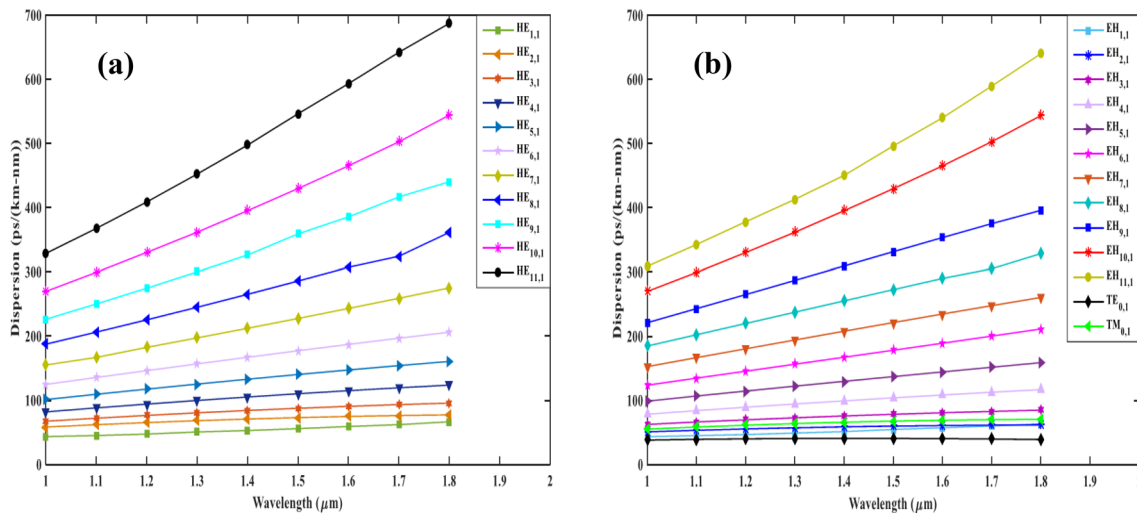
Fig. 4 Dispersion of different **a** HE modes, **b** EH, TE, and TM modes as a function of wavelength

dispersion equation. In the simulation of proposed PCF, it was verified that the effective refractive index is decreased by increasing operating wavelength and the identity relation between wavelength and dispersion is shown in Eq. (3). In Fig. 4a, b it is precisely displayed that dispersion is increased by raising the wavelength and the lower order OAM modes have a lower dispersion. Thus, the smooth dispersion variation is obtained for the use of fused silica as a cladding region because the fused silica has a small RI.

The dispersion variation of $HE_{1,1}$, $HE_{2,1}$, $HE_{3,1}$, $TM_{0,1}$, $TE_{0,1}$, $EH_{1,1}$, $EH_{2,1}$, and $EH_{3,1}$ are 23.049 ps/km nm, 18.9937 ps/km nm, 28.2265 ps/km nm, 15.2512 ps/km nm, 0.916 ps/km nm, 20.0409 ps/km nm, 10.8982 ps/km nm, and 22.1766 ps/km nm, respectively. As far we know, the dispersion variation 0.916 ps/km nm for $TE_{0,1}$ is the lower from the previous OAM related articles. Besides, the lower groups of the OAM modes obtain flat dispersion. Moreover, we also noticed in Fig. 4a, b that the dispersion variations of the HE mode is larger than the EH mode at the same order of OAM modes. Nonetheless, the higher groups of OAM modes are insecure in optical transmission. In this manner, the flat dispersion of a lower group of OAM modes is a strong candidate for stable fiber communication.

3.4 Confinement loss (CL)

Fiber losses will be produced at the time of transmitting light due to the internal absorption element properties, micro bending, and PCF design imperfection [18]. The confinement losses are exterminatory for optical communication. It is preceded by periodic cladding and well-organized air holes. The proposed PCF is constructed with a regular shape of cladding with the special size of air holes. Thus, the mediocre CL is obtained for the PCF. In the proposed

PCF, the average CL is gained about 10^{-7} dB/m for wavelength ranging from 1000 to 2000 nm and the lowest CL is 1.534×10^{-9} dB/m at operating wavelength 1400 nm for the $EH_{11,1}$ mode.

The CL is figured out by Eq. (4). It is directly correlated to the imaginary part of effective refractive indices and the obtained CL is plotted in Fig. 5. In the raised PCF, the CL variation of the different OAM modes is not linear compared to other parameters such as ERID, dispersion, numerical aperture, and nonlinearity, etc. because the values of CL is changed for a large wavelength difference (which is 0.1 μm in Fig. 5). For this reason, the graph displays larger zigzag trends, and also the same phenomenon was shown by the recently published articles [14, 15, 19]. The small confinement losses ensure the robust and efficient transmission of light in the fiber.

3.5 Effective refractive area and numerical aperture

The effective refractive area of the proposed PCF is mathematically calculated by Eq. (5). The calculation of the effective area is done in the simulation of the PCF. The effective area as a function of wavelength ranging from 1000 to 2000 nm is plotted in Fig. 6. Moreover, Fig. 6a shows all the HE modes and Fig. 6b shows all the EH modes and other Eigenmodes.

Another optical parameter, numerical aperture (NA) is reclined in an effective area. The NA is specialized by the total amount of optical capacity. It is a unit-less parameter of PCF. The NA is calculated through Eq. (6) The NA for all OAM modes is depicted in Fig. 7. According to the equation and figure, the NA is increased by increasing the wavelength. By comparing Figs. 6 and 7, it is found out that the
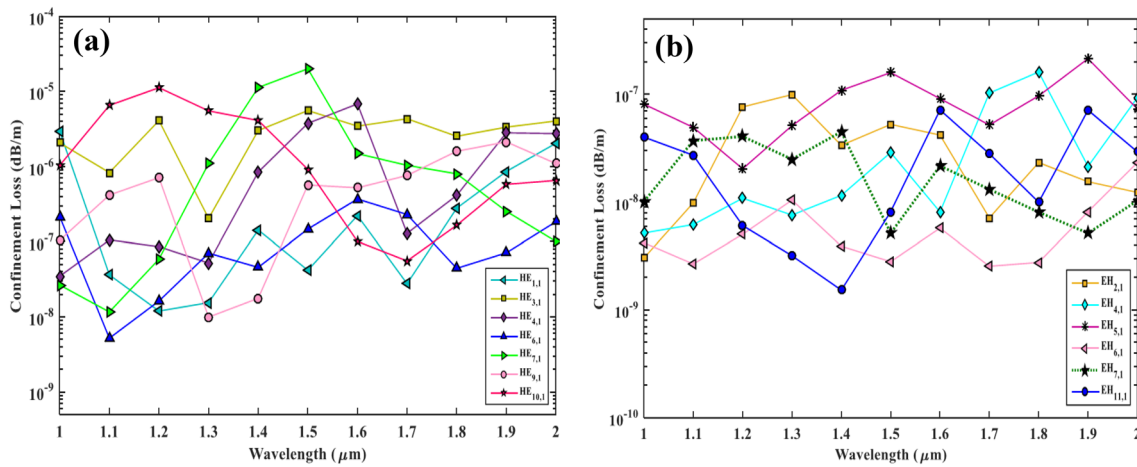
Fig. 5 Confinement loss of different **a** HE modes, **b** EH modes with respect to the wavelength
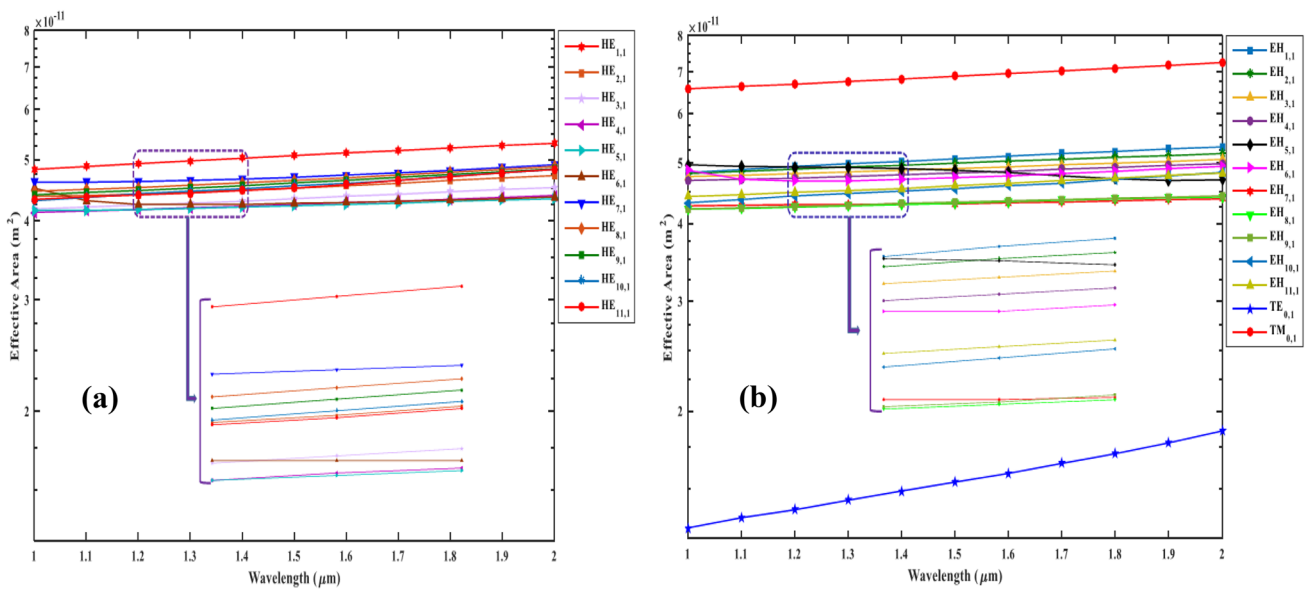

Fig. 6 The effective area of different **a** HE modes, **b** EH, TE, TM modes with respect to the wavelength

high profile of an effective area shows the low NA because both are inversely correlated. The proposed PCF shows the highest effective area for $TM_{0,1}$ mode and this area, the designed PCF has obtained the lowest NA. The fused silica is used as the background material of the proposed PCF. Silica is a material with a low refractive index. Thus, the PCF supports a low numerical aperture.

3.6 Nonlinearity

Nonlinearity is one of the most important parameters of the PCF. The nonlinearity of a PCF depends on the core size of the design. The nonlinearity is established a reverse relation with the core size and effective area of the PCF. The

proposed PCF has a larger center air-hole. The core size of the raised PCF provides a lower nonlinearity. The nonlinearity is mathematically calculated through Eq. (7) The nonlinearity of the proposed PCF is graphically shown in Fig. 8. The lowest nonlinearity of the PCF is 0.997 W^{-1} km^{-1} at wavelength 2000 nm for $TM_{0,1}$ mode. It can be achieved for the highest effective area 7.25×10^{-11} m^2 in the same situation as this mode. Moreover, the low nonlinear coefficient is advantageous for transmitting the OAM modes into optical fibers.

Table 1 shows the different parameters of PCF with a comparison. This table shows the performance between previous OAM related published articles and our proposed PCF.
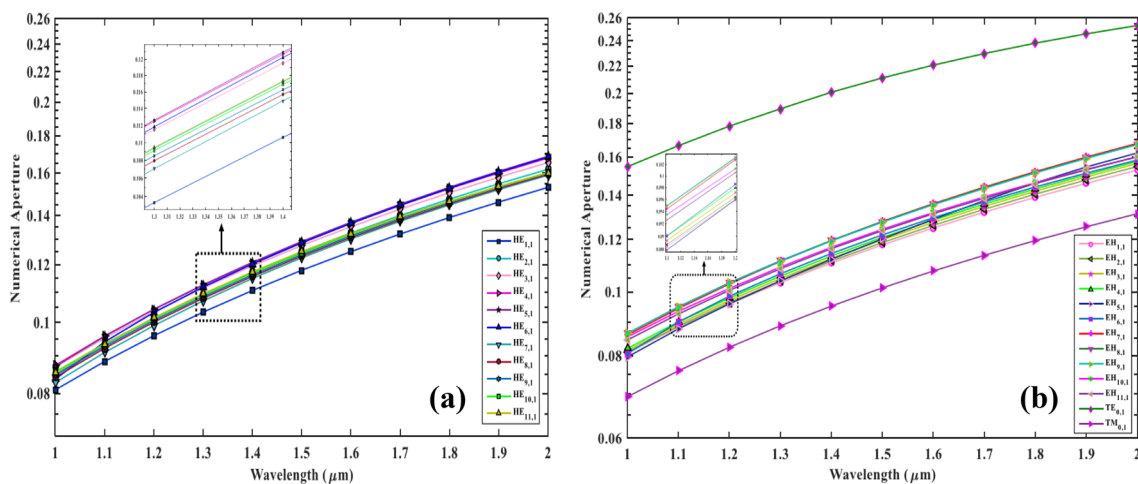
Fig. 7 The numerical aperture of different **a** HE modes, **b** EH, TE, TM modes with respect to the wavelength
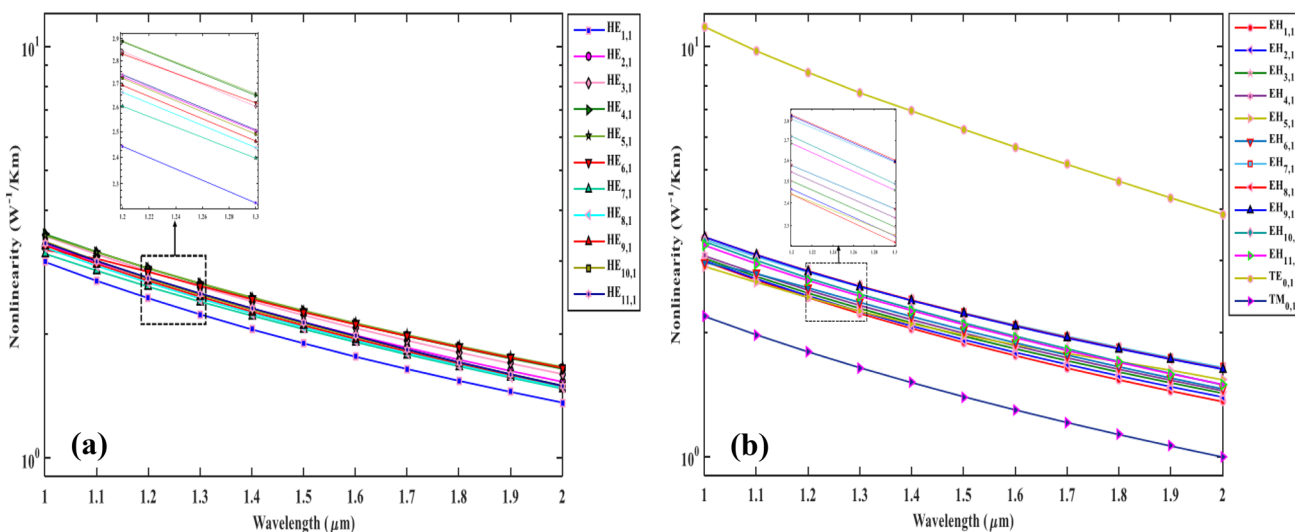

Fig. 8 Nonlinearity of different **a** HE modes, **b** EH, TE, and TM modes concerning the wavelength

Table 1 A comparison chart of structure type, bandwidth, dispersion variation, and confinement losses with the raised PCF and the recently published works

References	Structure type	Bandwidth (nm)	Dispersion variation of $TE_{0,1}$ (ps/km nm)	Confinement loss (dB/m)
[1]	Circular-PCF	100	–	$< 10^{-7}$
[10]	Spiral-PCF	> 600	10.35	5.0951×10^{-3}
[16]	Circular-PCF	750	< 46.38	3.434×10^{-9}
[18]	Double-PCF	850	–	$< 7 \times 10^{-9}$
[20]	Circular-PCF	560	–	9.52×10^{-9}
This work	**Circular-PCF**	**1000**	**0.916**	**1.534 × 10⁻⁹**

The bold indication referes to highlight the proposed work results

Thus, the proposed PCF is a strong candidate for OAM mode transmission and other related optical communications.

4 Conclusion

This article introduces a hollow larger center air-hole C-PCF with a new well-organized shape of air holes in the cladding region. Silica is used as a background element of this PCF. It can transmit data within a greater bandwidth (1000 nm) and supports up to 38 OAM modes with ensuring efficient transmission. All the propagation characteristics of the designed PCF are achieved by applying the FEM method and PML as a boundary condition through the COMSOL Multiphysics 4.3b simulator. It also prevents the linear polarization of adjacent vector modes. Additionally, this PCF has produced some special OAM features. In concise, the lowest dispersion variation and confinement loss is 0.916 ps/km nm for $TE_{0,1}$ mode and 1.534×10^{-9} dB/m for $EH_{11,1}$ mode at the operating wavelength of 1400 nm, respectively. Therefore, from the above analysis, this PCF ensures robust OAM mode transmission, and also other relevant optical communications with high capacity.

Compliance with ethical standards

Conflict of interest All the authors have read the manuscript and approved this for submission as well as no competing interests.

References

1. L. Zhang, K. Zhang, J. Peng, J. Deng, Y. Yang, J. Ma, Circular photonic crystal fiber supporting 110 OAM modes. Opt. Commun. **429**, 189–193 (2018)
2. M. Xu, G. Zhou, C. Chen, G. Zhou, Z. Sheng, Z. Hou, C. Xia, A novel microstructured fiber for OAM mode and LP mode simultaneous transmission. J. Opt. **47**(4), 428–436 (2018)
3. X. Zhang, H. Zhang, W. Tian, A circular photonic crystal fiber supporting OAM mode transmission. In 2016 15th International Conference on Optical Communications and Networks (ICOCN) (2016), pp. 1–3. IEEE
4. L. Allen, M.W. Beijersbergen, R.J.C. Spreeuw, J.P. Woerdman, Orbital angular momentum of light and the transformation of Laguerre–Gaussian laser modes. Phys. Rev. A **45**(11), 8185 (1992)
5. C. Jia, H. Jia, N. Wang, J. Chai, X. Xu, Y. Lei, G. Liu, Y. Peng, J. Xie, Theoretical analysis of a 750-nm bandwidth hollow-core ring photonic crystal fiber with a graded structure for transporting 38 orbital angular momentum modes. IEEE Access **6**, 20291–20297 (2018)
6. H. Huang, G. Milione, M.P. Lavery, G. Xie, Y. Ren, Y. Cao, N. Ahmed, T.A. Nguyen, D.A. Nolan, M.J. Li, M. Tur, Mode division multiplexing using an orbital angular momentum mode sorter and MIMO-DSP over a graded-index few-mode optical fibre. Sci. Rep. **5**, 14931 (2015)
7. K. Sueda, G. Miyaji, N. Miyanaga, M. Nakatsuka, Laguerre–Gaussian beam generated with a multilevel spiral phase plate for high intensity laser pulses. Opt. Express **12**(15), 3548–3553 (2004)
8. Y. Yan, G. Xie, M.P. Lavery, H. Huang, N. Ahmed, C. Bao, Y. Ren, Y. Cao, L. Li, Z. Zhao, A.F. Molisch, High-capacity millimetre-wave communications with orbital angular momentum multiplexing. Nat. Commun. **5**, 4876 (2014)
9. S. Li, J. Wang, Compensation of a distorted N-fold orbital angular momentum multicasting link using adaptive optics. Opt. Lett. **41**(7), 1482–1485 (2016)
10. A. Nandam, W. Shin, Spiral photonic crystal fiber structure for supporting orbital angular momentum modes. Optik **169**, 361–367 (2018)
11. X. Bai, H. Chen, H. Yang, Design of a circular photonic crystal fiber with square air-holes for orbital angular momentum modes transmission. Optik **158**, 1266–1274 (2018)
12. Y.E. Monfared, A. Mojtahedinia, A.M. Javan, A.M. Kashani, Highly nonlinear enhanced-core photonic crystal fiber with low dispersion for wavelength conversion based on four-wave mixing. Front. Optoelectron. **6**(3), 297–302 (2013)
13. B. Biswas, K. Ahmed, B.K. Paul, M.A. Khalek, M.S. Uddin, Numerical evaluation of the performance of different materials in nonlinear optical applications. Results Phys. **13**, 102184 (2019)
14. M.M. Hassan, M.A. Kabir, M.N. Hossain, B. Biswas, B.K. Paul, K. Ahmed, Photonic crystal fiber for robust orbital angular momentum transmission: design and investigation. Opt. Quantum Electron. **52**(1), 8 (2020)
15. M.A. Kabir, M.M. Hassan, M.N. Hossain, B.K. Paul, K. Ahmed, Design and performance evaluation of photonic crystal fibers of supporting orbital angular momentum states in optical transmission. Opt. Commun. **467**, 125731 (2020)
16. H. Zhang, W. Zhang, L. Xi, X. Tang, X. Zhang, X. Zhang, A new type circular photonic crystal fiber for orbital angular momentum mode transmission. IEEE Photonics Technol. Lett. **28**(13), 1426–1429 (2016)
17. H. Pakarzadeh, V. Sharif, Control of orbital angular momentum of light in optofluidic infiltrated circular photonic crystal fibers. Opt. Commun. **438**, 18–24 (2019)
18. N. Wang, J.L. Xie, H.Z. Jia, M.M. Chen, A low confinement loss double-photonic crystal fibre over 850 nm bandwidth with 26 orbital angular momentum modes transmission. J. Mod. Opt. **65**(18), 2060–2064 (2018)
19. M.F. Israk, M.A. Razzak, K. Ahmed, M.M. Hassan, M.A. Kabir, M.N. Hossain, B.K. Paul, V. Dhasarathan, Ring-based coil structure photonic crystal fiber for transmission of orbital angular momentum with large bandwidth: outline, investigation and analysis. Opt. Commun. **473**, 126003 (2020)
20. H. Zhang, X. Zhang, H. Li, Y. Deng, X. Zhang, L. Xi, X. Tang, W. Zhang, A design strategy of the circular photonic crystal fiber supporting good quality orbital angular momentum mode transmission. Opt. Commun. **397**, 59–66 (2017)